Journal of Porous Media, 2(1), 39–58 (1999)

Free Convective Boundary Layer Flow from a Heated Surface in a Layered Porous Medium

D. A. S. Rees

School of Mechanical Engineering, University of Bath, Claverton Down, Bath BA2 7AY, U.K.

ABSTRACT

We examine theoretically the steady free convective flow from an isothermal vertical flat plate embedded in a saturated porous medium. We consider in detail the effect of parallel layering on the flow and rate of heat transfer. The layering arises from discrete changes in either the permeability or the diffusivity of the porous medium. Mathematically, the presence of layering causes the boundary layer equations to be non-similar, and these equations are solved numerically using the Keller-box method. The numerical work is supplemented by an asymptotic analysis of the flow in the far-downstream limit. Where there is a finite number of sublayers sandwiched between the heated surface and the remaining isotropic medium, detailed results are limited by the appearance of eigensolutions in the asymptotic expansion. When the medium is composed of alternating sublayers an asymptotic analysis yields an equivalent homogeneous medium.

Received September 5, 1996; Accepted April 9, 1997

INTRODUCTION

This article presents an analysis of free convection boundary layer flow from heated surfaces in a layered porous medium. Studies of the effects of layering and of boundary layer flows have until now followed their own entirely distinct courses. Neither area has a particularly large volume of published research devoted to it and we present a brief review of much of this.

Convection in layered media has concentrated exclusively on finite containers or on layers of infinite horizontal extent heated from below. Examples of the former are found in articles by McKibbin (1986), Poulikakos and Bejan (1983), and Lai and Kulacki (1988). McKibbin examined the onset of convection in a layered container heated from below whereas the other authors concentrated on side-wall heating configurations where convective motions always occur. In the above-quoted studies, both vertical and horizontal layering was considered. A slightly more substantial theory exists for the layered porous equivalent of the Bénard problem. Georghitza (1961) was the first to consider the effects of inhomogeneities, closely followed by Donaldson (1962), who considered a two-layer system. Masuoka et al. (1978) derived criteria for the onset of convection and proceeded to compute some strongly nonlinear two-dimensional flows. Rana et al. (1979) used a three-layer system to model the Pahoa reservoir in Hawaii. A comprehensive analysis of the onset of convection and the subsequent weakly nonlinear heat transfer of two-dimensional flow was presented by McKibbin and O'Sullivan (1980, 1981). This was extended subsequently to systems with very thin, highly impermeable sheets (McKibbin and Tyvand, 1983) and very thin highly permeable cracks (McKibbin and Tyvand, 1984). McKibbin (1983) also generalized Donaldson's work, and has very recently considered the effects of inclination and anisotropic sublayers on the onset of convection (Trew and McKibbin, 1994). An examination of the assumption of two-dimensionality used by McKibbin and O'Sullivan (1981) was undertaken by Rees and Riley (1990), who found the criteria governing when the preferred flow patterns are three-dimensional. This reference also contains detailed results on the ranges of stable wavenumbers.

The first studies on thermal boundary layer flow in a porous medium were conducted by Cheng and Minkowycz (1977) for the vertical heated surface and by Cheng and Chang (1976) for the horizontal surface. Many authors have extended these analyses by considering separately power-law temperature distributions, prescribed rates of surface heat flux, surface suction, non-Newtonian flow, anisotropy, and radiation effects; further details may be found in the monograph by Nield and Bejan (1992). The main emphasis in this paragraph is on the stability and hence the realizability of the boundary layer flows in practice. Hsu et al. (1978) and Hsu and Cheng (1979) considered the stability of horizontal and inclined boundary layers to small-amplitude disturbances forming a spanwise vortex system. Using the parallel flow approximation Hsu and Cheng found that the distance from the leading edge beyond which disturbances grow (expressed in their article in terms of a local Darcy—Rayleigh number) increases without bound as the inclination of the upward-facing surface nears the vertical. A recent article by Storesletten and Rees (1996) used high-order boundary layer theory of the type used by Chang and Cheng (1983), Cheng and Hsu (1984), and Daniels and Simpkins (1984) to provide the basic flow for a vortex stability analysis. Storesletten and Rees (1998) found that the results of Hsu and Cheng are reliable only at angles fairly close to the vertical because the leading order boundary layer flow inadequately represents the true flow at smaller angles from the horizontal. However, the basic result that the vertical boundary layer is stable is confirmed.

It is necessary also to consider wavelike disturbances, for Gill's (1969) analysis of the vertical channel heated from the side shows that Squire's theorem applies, implying that two-dimensional disturbances are more important than those that are three-dimensional. This fact motivated the direct numerical simulation of Rees (1993) and the asymptotic analysis of Lewis et al. (1995), both of which considered uniformly heated surfaces. The former article demonstrates that even large-amplitude disturbances decay in a large but necessarily finite computational domain. The latter gives precise growth rates for wavelike disturbances at asymptotically large distances from the leading edge. Although the absolute value of the growth rate decreases, it always remains negative and therefore disturbances decay. Taken together, these articles give a very strong argument for the stability of the vertical boundary layer.

In this article we consider the effect of layering on the flow and rate of heat transfer from a uniformly heated vertical surface embedded in a porous medium. We consider a vertical surface because the results described in the last two paragraphs indicate that it is probable that such a flow will be stable and therefore will be seen in practice. The sublayers comprising the porous medium are aligned such that the interfaces are parallel with the heated surface. This is, of course, not the only alignment of interfaces with respect to the heated surface, and these other cases will be reported in due course. In particular we consider

three different types of configuration displaying layering. The first consists of one sublayer sandwiched between the heated surface and the rest of the medium which is uniform and isotropic. The second has two such sublayers and the third is composed of an infinite number of sublayers with alternating properties. In all three cases we present finite-difference computations of the resulting nonsimilar boundary layer flows using suitably modified versions of the Keller-box method. The numerical simulations are supplemented by detailed asymptotic analyses for large distances from the leading edge.

GOVERNING EQUATIONS

In this article we study the effects of discrete layering on the free convection boundary layer flow from a heated vertical surface in a porous medium. Three different types of media are examined in detail: (1) a uniform medium with a single sublayer placed adjacent to the heated surface; (2) a uniform medium with two such sublayers; and (3) a medium composed of layers with alternating properties. The governing equations described below are those corresponding to the first configuration—modifications for the second and third are detailed at the appropriate places in the text.

Consider a semiinfinite vertical surface with constant temperature, T_w, embedded in a fluid-saturated porous medium with ambient temperature, T_∞. The permeability and thermal diffusivity of the medium are constant and equal to K_2 and κ_2, respectively when $\hat{y} > 0$, where $\hat{y}$ is the dimensional coordinate perpendicular to the heated surface. The heated surface is situated at $\hat{y} = -d$ for $\hat{x} > 0$, where $\hat{x}$ is the dimensional coordinate measured upwards from the leading edge of the heated surface. In the region lying between $\hat{y} = -d$ and $\hat{y} = 0$ there is a porous layer with permeability K_1 and diffusivity κ_1; these values may or may not be different from K_2 and κ_2, respectively. The full steady, two-dimensional Darcy–Boussinesq equations that are satisfied are given by

$$\frac{\partial \hat{u}_i}{\partial \hat{x}} + \frac{\partial \hat{v}_i}{\partial \hat{y}} = 0 \tag{1a}$$

$$\hat{u}_i = -\frac{K_i}{\mu}\left(\frac{\partial \hat{p}_i}{\partial \hat{x}} - \rho\beta(T_i - T_\infty)g\right) \tag{1b}$$

$$\hat{v}_i = -\frac{K_i}{\mu}\left(\frac{\partial \hat{p}_i}{\partial \hat{y}}\right) \tag{1c}$$

$$\hat{u}_i \frac{\partial T_i}{\partial \hat{x}} + \hat{v}_i \frac{\partial T_i}{\partial \hat{y}} = \kappa_i\left(\frac{\partial^2 T_i}{\partial \hat{x}^2} + \frac{\partial^2 T_i}{\partial \hat{y}^2}\right) \tag{1d}$$

Here ρ, β, and μ are the density, the coefficient of cubical expansion, and viscosity of the saturating fluid, and g is gravity. The subscript i denotes which layer is being considered: $i = 1$ corresponds to the near-wall layer, termed region 1, and $i = 2$ to the rest of the medium, called region 2. At the heated surface, $\hat{y} = -d$, the boundary conditions are that

$$\hat{v}_1 = 0 \quad \text{and} \quad T_1 = T_w \tag{2a}$$

where $T_w > T_\infty$, and as $y \to \infty$

$$\hat{u}_2 \to 0 \quad \text{and} \quad T_2 \to T_\infty \tag{2b}$$

At the interface, $\hat{y} = 0$, the normal velocity, temperature, rate of heat transfer, and pressure need to be continuous and hence

$$\hat{v}_1 = \hat{v}_2, \quad T_1 = T_2, \quad k_1 \frac{\partial T_1}{\partial \hat{y}} = k_2 \frac{\partial T_2}{\partial \hat{y}}, \quad \text{and} \quad \hat{p}_1 = \hat{p}_2 \tag{2c}$$

Here, $k_i = \rho c \kappa_i$ is the thermal conductivity of layer i, and c is the heat capacity of the saturating fluid.

The above equations and boundary conditions may be nondimensionalized, but we use a different nondimensionalization from that given in previous studies (Daniels and Simpkins, 1984; Riley and Rees, 1985; Rees and Storesletten, 1995) because we have a natural length scale available, namely, the width of the sublayer near the heated surface. Therefore we introduce the following scalings:

$$(x, y) = d(\hat{x}, \hat{y}), \quad T_i = T_\infty + (T_0 - T_\infty)\theta_i \tag{3a, b}$$

$$(u_i, v_i) = \left(\frac{\kappa_2}{d}\right)(\hat{u}_i, \hat{v}_i) \tag{3c}$$

into Eqs. (1) and (2). Because the flow is two-dimensional the resulting nondimensional equations may be simplified further by introducing the streamfunction, ψ_i, according to

$$u_i = \frac{\partial \psi_i}{\partial y}, \quad v_i = -\frac{\partial \psi_i}{\partial x} \tag{4}$$

Hence we obtain the following set of equations:

$$\frac{\partial^2 \psi_i}{\partial x^2} + \frac{\partial^2 \psi_i}{\partial y^2} = R\left(\frac{K_i}{K_2}\right)\frac{\partial \theta_i}{\partial y} \tag{5a}$$

$$\frac{\kappa_i}{\kappa_2}\left(\frac{\partial^2 \theta_i}{\partial x^2} + \frac{\partial^2 \theta_i}{\partial y^2}\right) = \frac{\partial \psi_i}{\partial y}\frac{\partial \theta_i}{\partial x} - \frac{\partial \psi_i}{\partial x}\frac{\partial \theta_i}{\partial y} \tag{5b}$$

with the boundary conditions

$$\psi_1 = 0, \quad \theta_1 = 1, \quad \text{on} \quad y = -1 \ (x > 0) \tag{5c}$$

$$\frac{\partial \psi_2}{\partial y}, \theta_2 \to 0 \quad \text{as} \quad y \to \infty \tag{5d}$$

and interface conditions on $y = 0$

$$\psi_1 = \psi_2, \quad K_2\frac{\partial\psi_1}{\partial y} = K_1\frac{\partial\Psi_2}{\partial y}, \quad \theta_1 = \theta_2, \quad \text{and}$$

$$\kappa_1\frac{\partial\theta_1}{\partial y} = \kappa_2\frac{\partial\theta_2}{\partial y} \tag{5e}$$

In Eq. (5a) the Darcy–Rayleigh number, defined by

$$R = \frac{\rho g\beta(T_0 - T_\infty)K_2 d}{\mu\kappa_2} \tag{6}$$

is based on the permeability and diffusivity of region 2, and therefore the near-wall layer, region 1, is regarded as an imperfection in an otherwise homogeneous and isotropic medium.

In the three-layer configuration, where there are two sublayers (regions 1 and 2) sandwiched between the main medium (region 3) and the vertical surface, we shall assume that the first and third regions have identical properties, and shall base the Rayleigh number on K_1 and κ_1. Thus region 2 is regarded as the imperfection in the otherwise homogeneous medium. In the multiply layered medium the sublayers are assumed to have alternating properties, and therefore we base the Rayleigh number on K_1 and κ_1.

The boundary layer approximation is now invoked by assuming that the Darcy–Rayleigh number is large. In studies of this kind, where the dimensional length scale is arbitrary, it is usual to assume that $x = O(1)$ defines the nondimensional distance downstream of the leading edge that is of interest. A simple scaling argument is then used to show that $y = O(R^{-1/2})$ is the boundary layer thickness. For the present problem such an analysis would yield a similarity solution because the boundary layer is asymptotically thinner than the width of the sublayer corresponding to region 1: $y = O(1)$. Therefore it is necessary to look at much larger values of x, and, in particular, at those values that correspond to an $O(1)$ boundary layer thickness, for this is when the effect of layering modifies the boundary layer flow. Assuming then that $y = O(1)$ in the boundary layer, the scaling argument can again be used to show that $x = O(R)$ is the appropriate downstream distance to be considered. Given that region 1 has constant thickness, and bearing in mind that the streamfunction grows like $x^{1/2}$ when the porous medium is homogeneous, we introduce the following transformation:

$$\psi_1 = R\xi^{1/2}F^{(1)}(y, \xi), \quad \theta_1 = G^{(1)}(y, \xi) \quad \text{where} \quad x = R\xi \tag{7}$$

If we let $R \to \infty$ and retain leading-order terms then the region 1 boundary layer equations are found to be

$$F^{(1)}_{yy} = \left(\frac{K_1}{K_2}\right)\xi^{-1/2}G^{(1)}_y \tag{8a}$$

$$\left(\frac{\kappa_1}{\kappa_2}\right)G^{(1)}_{yy} + \frac{1}{2}\xi^{-1/2}F^{(1)}G^{(1)}_y = \xi^{1/2}(F^{(1)}_y G^{(1)}_\xi - F^{(1)}_y G^{(1)}_\xi) \tag{8b}$$

For sufficiently large values of ξ it is to be expected that the boundary layer will extend well into region 2 and its shape will begin to resemble that of the homogeneous self-similar boundary layer. Therefore we transform the full equations using the following substitutions:

$$\psi_2 = R\xi^{1/2}F^{(2)}(\eta, \xi), \quad \theta_2 = G^{(2)}(\eta, \xi) \tag{9a, b}$$

where

$$\eta = R^{1/2}y/x^{1/2} \tag{9c}$$

Hence the region 2 boundary layer equations are

$$F^{(2)}_{\eta\eta} = G^{(2)}_\eta \tag{10a}$$

$$G^{(2)}_{\eta\eta} + \frac{1}{2}F^{(2)}G^{(2)}_\eta = \xi(F^{(2)}_\eta G^{(2)}_\xi - F^{(2)}_\xi G^{(2)}_\eta) \tag{10b}$$

The boundary and interface conditions are now given by

$$F^{(1)} = 0, \quad G^{(1)} = 1 \quad \text{at} \quad y = -1 \tag{11a}$$

$$F^{(2)}_\eta \to 0, \quad G^{(2)} \to 0 \quad \text{as} \quad \eta \to \infty \tag{11b}$$

and

$$F^{(1)} = F^{(2)}, \quad K_2F^{(1)}_y = K_1\xi^{-1/2}F^{(2)}_\eta \tag{12a, b}$$

$$G^{(1)} = G^{(2)}, \quad \kappa_1G^{(1)}_y = \kappa_2\xi^{-1/2}G^{(2)}_\eta \tag{12c, d}$$

on $y = \eta = 0$. The corresponding equations for the two-sublayer and multilayer configurations may be derived in almost identical fashion, and they are quoted later.

The rate of heat transfer from the heated surface is of significance, and it is important to know how the presence of layering modifies the heat loss when compared with that corresponding to a uniform medium. The local rate of heat transfer, q, is given by

$$q = -k_1\frac{\partial T_1}{\partial\hat{y}} = -\frac{k_1(T_w - T_\infty)}{d}\frac{\partial\theta_1}{\partial y} \tag{13}$$

at the heated surface. When ξ is sufficiently small, the boundary layer is contained well within the near-wall layer, and the flow is essentially self-similar with exponentially small errors. Thus $F^{(1)}$ and $G^{(1)}$ take the form

$$F^{(1)}(y, \xi) \sim \left(\frac{\kappa_1K_1}{\kappa_{\text{ref}}K_{\text{ref}}}\right)^{1/2} f(\zeta), \quad G^{(1)}(y, \xi) \sim g(\zeta) \tag{14a}$$

where

$$\zeta = \left(\frac{\kappa_{\text{ref}} K_1}{\kappa_1 K_{\text{ref}}}\right)^{1/2} (y+1)/\xi^{1/2} \tag{14b}$$

and where $f(\zeta)$ and $g(\zeta)$ satisfy

$$f''' = g', \quad g'' + \frac{1}{2} f g' = 0 \tag{15a}$$

subject to

$$f(0) = 0, \; g(0) = 1, \text{ and } f', g \to 0 \text{ as } \zeta \to \infty \tag{15b}$$

see Cheng and Minkowycz (1977). In Eq. (14) we have retained a slightly more general expression by not specifying which layer is being treated as the reference layer. Near the leading edge, the local rate of heat transfer is given by

$$q = -\frac{k_{\text{ref}}(T_w - T_\infty)}{d} \left(\frac{\kappa_{\text{ref}} K_1}{\kappa_1 K_{\text{ref}}}\right)^{1/2} \xi^{-1/2} g'(0) \tag{16}$$

and therefore a suitable scaled rate of heat transfer is Q, where

$$Q = \frac{q d \xi^{1/2}}{k_{\text{ref}}(T_w - T_\infty)} = -\left(\frac{\kappa_{\text{ref}}}{\kappa_1}\right) \xi^{1/2} \frac{\partial G^{(1)}}{\partial y} \tag{17}$$

at the heated surface. Near the leading edge this relationship reduces to

$$Q \sim -\left(\frac{\kappa_{\text{ref}} K_1}{\kappa_1 K_{\text{ref}}}\right)^{1/2} g'(0) \tag{18}$$

where the value of $g'(0)$ is computed to be

$$g'(0) = -0.44375 \tag{19}$$

NUMERICAL SOLUTION FOR ONE SUBLAYER

Equations (8) and (10), together with the boundary and interface conditions [Eqs. (9) and (11)], are nonsimilar unless $K_1 = K_2$ and $\kappa_1 = \kappa_2$. We have therefore employed the Keller-box method to integrate numerically from very near the leading edge to a position well downstream. The presence of layering makes the application of the Keller-box method somewhat more involved than is usual and therefore we shall describe our implementation in detail. Very near the leading edge, but still within the regime, $\xi = O(1)$, the boundary layer is only just beginning to develop and its thickness is considerably less than the thickness of the near-wall layer. For such values of ξ the boundary layer flow is essentially self-similar and is given by Eq. (13). Any errors in the solution here will be very small because the solution decays exponentially. Indeed when $\zeta = 20$, say, the differences between the values of f' and g and the corresponding values at $\zeta = \infty$ is less than 10^{-6} in absolute terms. Therefore we begin the Keller-box computation at that value of ξ for which $\zeta = 20$ corresponds precisely to $y = 0$, the interface between the two regions. The starting profile is not computed using an alternative method, such as a Runge–Kutta scheme, but rather the Keller-box code itself is used to solve the governing ordinary differential equations.

In our implementation we used a total of 111 unevenly spaced points in the y or η directions that lie in the ranges $-1 \le y \le 0$ and $0 \le \eta \le 20$; 61 of these lay in the former range to represent the solution sufficiently accurately when ξ is small and the boundary layer is thin, and the remainder were needed to represent the solution well for large values of ξ. The points in the ξ direction took the form $\xi_k = \xi_{\min} + \delta_k$ where $\xi_{\min}$ is the initial value of ξ described previously, and δ_k formed a geometric series from $\delta_1 = 0.0001$ to $\delta_{161} = 10000.0$; i.e., $\delta_k = 10^{-4+[(k-1)/20]}$.

Equations (8) and (10) were discretized centrally in y and η, respectively, and the interface conditions [Eq. (11c)] regarded simply as another set of equations to be satisfied. When the interface conditions were placed in the appropriate place in the equivalent Newton–Raphson iteration scheme that forms part of the Keller-box method, the Jacobian matrix retains its tridiagonal structure. However, we found that the usual central difference approximation in the ξ direction gives rise to large but bounded oscillations in the numerical solutions. The oscillations reduce in magnitude as the ξ step is reduced, but their entire elimination requires an extremely small streamwise steplength. Therefore it was decided to use a backward difference modification to the Keller-box method and the solutions obtained, though now formally only first-order accurate in ξ, showed no sign of oscillations even for large steplengths. The implementation was tested by solving the full system of boundary layer equations for the case $K_1 = K_2$ and $\kappa_1 = \kappa_2$. The solution obtained should be the self-similar solution of Cheng and Minkowycz (1977) and therefore quantities such as $F^{(2)}(\eta = \eta_{\max})$ and $\xi^{-1/2} \partial G^{(1)} / \partial y \,|\, (y = -1)$ should remain constant. As the equations are formulated on a composite region it is to be expected that these quantities should vary to some extent, for the boundary layer develops in region 1 and grows in width there. However, variations in these test quantities were very small indeed and this lent confidence in the accuracy and integrity of the code. Ease of coding was obtained by employing numerical differentiation to obtain the Jacobian matrix, rather than by specifying it directly.

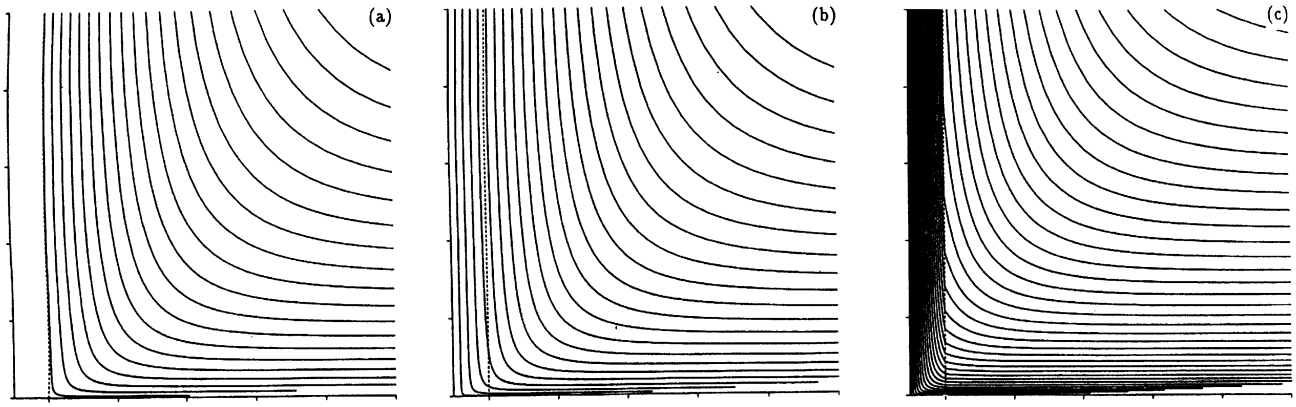

Figure 1. Streamlines corresponding to the cases (a) $K_1/K_2 = 0.2$, (b) $K_1/K_2 = 1$, and (c) $K_1/K_2 = 5$; in all cases $\kappa_1 = \kappa_2$. The streamlines are at intervals of 0.2—this applies to all figures displaying streamlines in the paper. Tickmarks on the axes are at an interval of 2 and the interface between regions 1 and 2 is displayed as a dashed line.

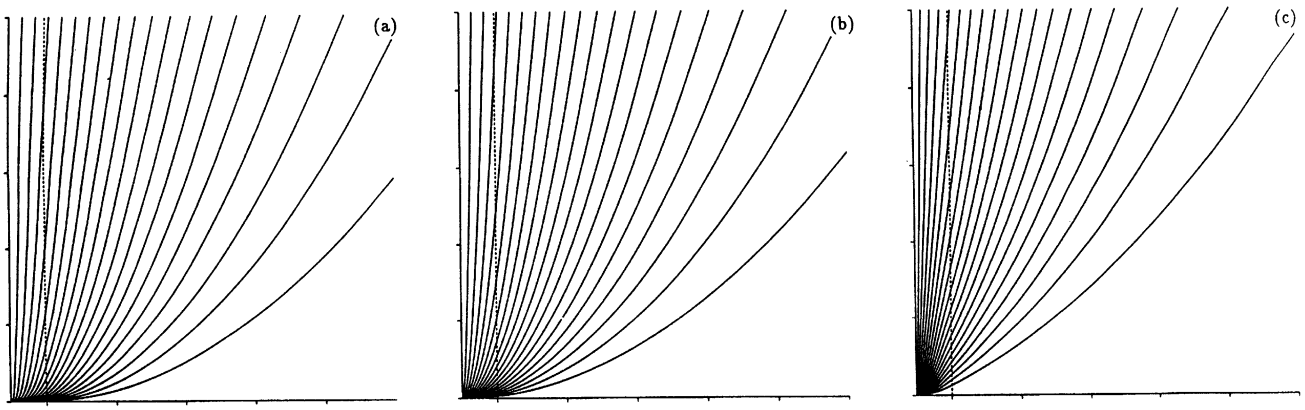

Figure 2. Isotherms corresponding to the cases displayed in Fig. 1. The isotherms are at intervals of 0.05—this applies to all figures in the article displaying isotherms. Tickmarks on the axes are at an interval of 2 and the interface between regions 1 and 2 is displayed as a dashed line.

Figures 1a,b,c and 2a,b,c show the effect of different permeability ratios, K_1/K_2, on the streamlines and isotherms. Figures 1b and 2b represent the datum case where $K_1 = K_2$ and $\kappa_1 = \kappa_2$, for which the flow is self-similar. When $K_1 = K_2/5$, as shown in Figs. 1a and 2a, the fluid is inhibited from moving quickly in region 1, and therefore the heat lost from the surface by advection is reduced. Consequently the boundary layer grows relatively quickly in thickness when compared with the datum case—compare Figs. 2a and 2b near $\xi = 0$. Once the growing boundary layer encounters the relatively permeable region 2 buoyancy forces meet with less resistance and therefore the streamwise velocity increases. This brings about an increased heat transfer by advection. The opposite occurs when $K_1 = 5K_2$ where the greatly increased near-wall permeability causes an enhanced fluid motion compared with the datum case, thereby thinning the boundary layer, as seen by comparing Figs. 2b and 2c. Much further downstream, where most of the boundary layer occupies region 2, the boundary layers are of comparable width, and the presence of a near-wall sublayer serves only to perturb slightly the shape of the boundary layer and its rate of heat transfer.

It should be noted that the discontinuous slopes of the streamlines in Fig. 1c are due to the interface conditions—

although the normal flux velocity must be continuous on physical grounds, the tangential flux velocity cannot be continuous as the order of the governing partial differential equations is insufficiently high to allow this. Such discontinuities in layered media have also been noted by McKibbin and O'Sullivan (1980, 1981) and Rees and Riley (1990).

Figures 3a,b and 4a,b show the effects of different diffusivity ratios on the temperature and flow fields while keeping $K_1 = K_2$. Figures 3a and 4a correspond to the case $\kappa_1 = \kappa_2/5$. In this case the boundary layer near the leading edge is relatively thin as the heat transfer is inhibited. However, when the temperature field eventually penetrates into region 2, the boundary layer grows more rapidly in thickness than near the leading edge. Figure 3a shows this clearly, and the discontinuous slope of the isotherms reflects the discontinuity in conductivity at the interface. Figures 3b and 4b correspond to the case $\kappa_1 = 5\kappa_2$. Now the boundary layer grows very quickly near the leading edge because of the enhanced diffusivity there. This growth is inhibited when the temperature field spreads into region 2. The rapid boundary layer growth near the leading edge is accompanied by high fluid fluxes as shown by the close spacing of the streamlines in Fig. 4b as compared with the datum case (Fig. 1b) and with the $\kappa_1 = \kappa_2/5$ case shown in Fig. 4a.

The above flows and others are summarized in Figs. 5 and 6, which show the variation with ξ of the scaled rate of heat transfer, Q. Figure 5 corresponds to cases with different permeability ratios where the diffusivities are

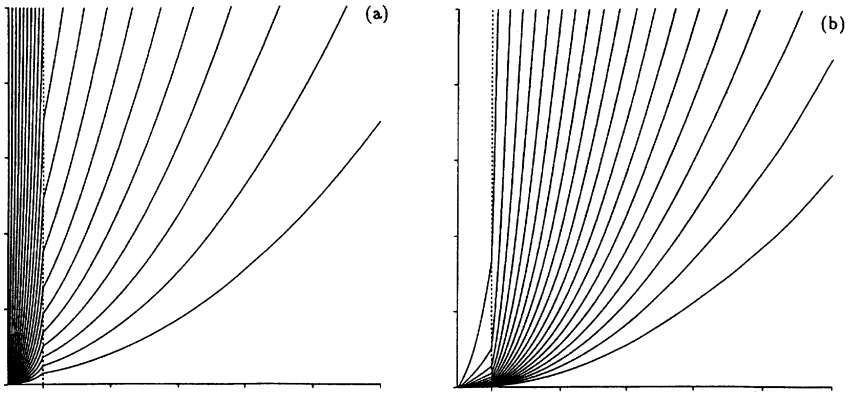

Figure 3. Isotherms corresponding to the cases (a) $\kappa_1/\kappa_2 = 0.2$, (b) $\kappa_1/\kappa_2 = 5$; in both cases $K_1 = K_2$.

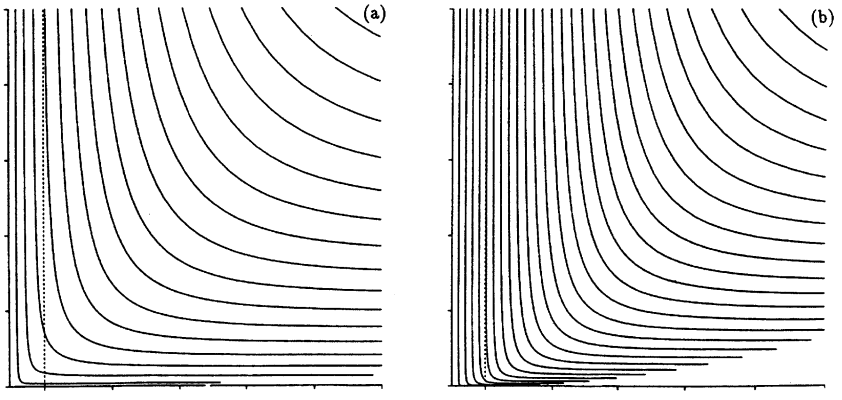

Figure 4. Streamlines corresponding to the cases displayed in Fig. 3.

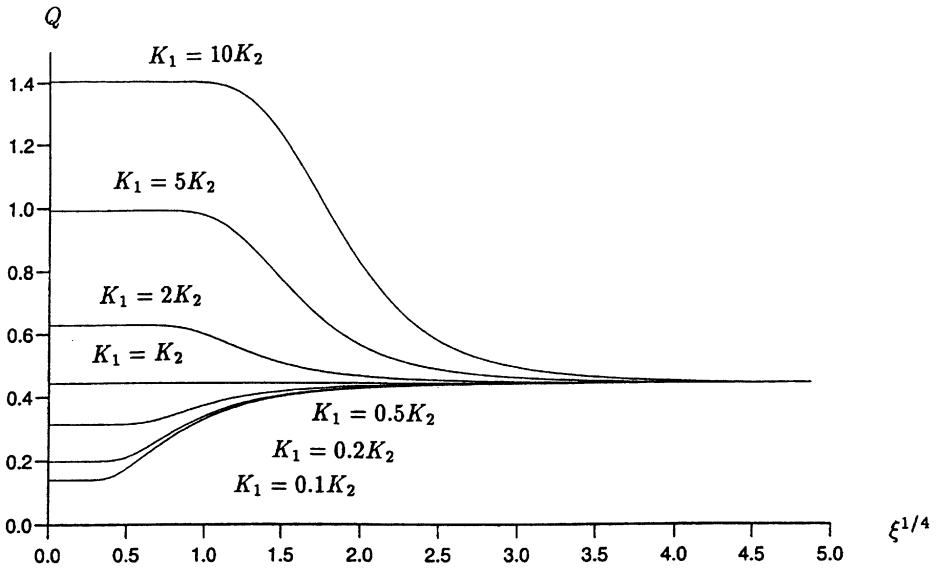

Figure 5. Values of Q, the scaled rate of heat transfer given by Eq. (17), for different permeability rations with $\kappa_1 = \kappa_2$.

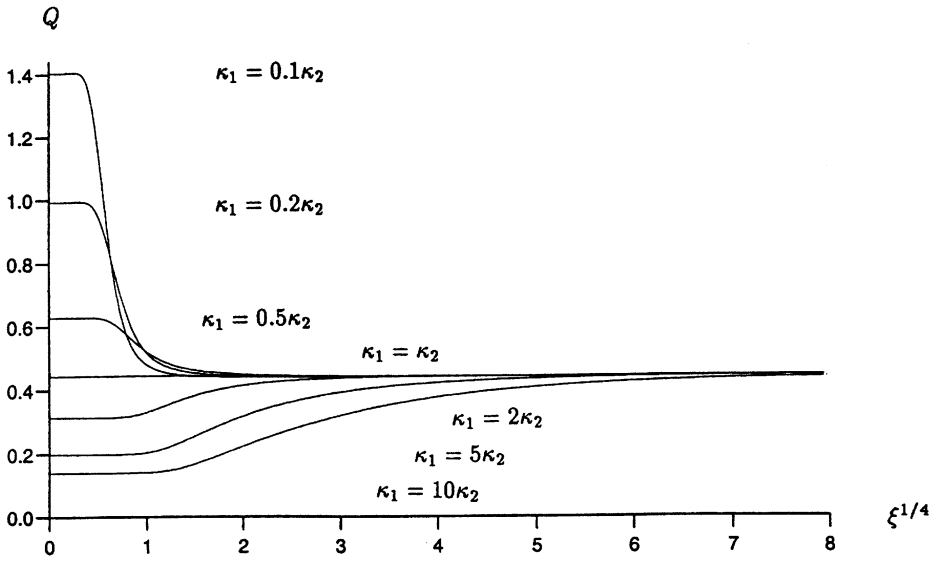

Figure 6. Values of Q, the scaled rate of heat transfer given by Eq. (17), for different diffusivity ratios with $K_1 = K_2$.

identical. For small values of ξ, Q is given by Eq. (18), and this is confirmed by the numerical results. For all permeability ratios, Q varies monotonically as ξ increases and it eventually asymptotes to the uniform medium value, $g'(0)$, when ξ is large. The manner in which Q approaches the common asymptotic value is investigated in the next section. The behavior of Q for different diffusivity ratios when $K_1 = K_2$ is shown in Fig. 6. Again, the small-ξ value given in Eq. (18) is reproduced in the graphs, and the large-ξ values asymptote to the same constant.

ASYMPTOTIC SOLUTION FOR ONE SUBLAYER

In this section we present an analysis of the boundary layer at asymptotically large distances from the leading edge. In particular we shall attempt to verify the behavior of the numerical solutions in this limit. It is clear from the numerical evidence that the flow tends toward the uniform medium self-similar solution as ξ increases, that is, $F^{(2)} \sim f(\eta)$ and $G^{(2)} \sim g(\eta)$. Given the form of the interface conditions [Eq. (11)], we expand the solution in powers of $\xi^{-1/2}$, at least initially. We find that the appropriate form of the asymptotic expansion is

$$F^{(1)} = \xi^{-1/2}F_1^{(1)} + \xi^{-1}F_2^{(1)} + \xi^{-3/2}\ln\xi F_3^{(1)} + \xi^{-3/2}F_3^{(1)} + \ldots \quad (20a)$$

$$G^{(1)} = 1 + \xi^{-1/2}G_1^{(1)} + \xi^{-1}G_2^{(1)} + \xi^{-3/2}\ln\xi\tilde{G}_3^{(1)} + \xi^{-3/2}G_3^{(1)} + \ldots \quad (20b)$$

$$F^{(2)} = f(\eta) + \xi^{-1/2}F_1^{(2)} + \xi^{-1}\ln\xi\tilde{F}_2^{(2)} + \xi^{-1}F_2^{(2)} + \ldots \quad (20c)$$

$$G^{(2)} = g(\eta) + \xi^{-1/2}G_1^{(2)} + \xi^{-1}\ln\xi\tilde{G}_2^{(2)} + \xi^{-1}G_2^{(2)} + \ldots \quad (20d)$$

Beginning with the first terms in Eqs. (20c) and (20d), the initial conditions [Eq. (11a)], and interface conditions, [Eqs. (12b) and (12d)], are used to solve for the first terms in the region 1 solution. These are,

$$F_1^{(1)} = \frac{K_1}{K_2}(1+y), \quad G_1^{(1)} = \frac{\kappa_2}{\kappa_1}g'(0)(1+y) \quad (21a, b)$$

The next terms in region 2 are obtained by applying the interface conditions, Eqs. (12a) and (12c), and the boundary conditions, Eq. (11b); thus $F_1^{(2)}$ and $G_1^{(2)}$ are found to be

$$F_1^{(2)} = \frac{K_1}{K_2} + \frac{\kappa_2}{\kappa_1}g'(0)\int_0^\eta \exp\left[-\frac{1}{2}\int_0^{\lambda_1} f(\gamma_2)\,d\gamma_2\right]d\gamma_1 \quad (22a)$$

$$G_1^{(2)} = \frac{\kappa_2}{\kappa_1}g'(0)\exp\left[-\frac{1}{2}\int_0^\eta f(\gamma_2)\,d\gamma_2\right] \quad (22b)$$

After a little manipulation with various equations, it is possible to show that Eqs. (22a) and (22b) may be rewritten in the much simpler form

$$F_1^{(2)} = \left(\frac{K_1}{K_2} - \frac{\kappa_2}{\kappa_1}\right) + \frac{\kappa_2}{\kappa_1}g(\eta), \quad G_1^{(2)} = \frac{\kappa_2}{\kappa_1}g'(\eta) \quad (22c, d)$$

This process of applying the interface conditions to obtain successive solutions may be continued, and the next terms in region 1 are

$$F_2^{(1)} = \frac{1}{2}\frac{\kappa_2 K_1}{\kappa_1 K_2}g'(0)(1+y)^2, \quad G_2^{(1)} = 0 \quad (23a, b)$$

Because we are interested in determining rates of heat transfer, Eq. (23b) shows that the leading order correction to that given by Eq. (21b) does not arise at $O(\xi^{-1/2})$. We are therefore forced to $O(\xi^{-1})$. It turns out, however, that a naive expansion in terms of inverse powers of $\xi^{-1/2}$ is incorrect as eigensolutions make their first appearance at this stage: this is the reason for including logarithmic terms in Eq. (20).

At $O(\xi^{-1}\ln\xi)$ the governing equations are

$$\tilde{F}_{2\eta\eta}^{(2)} = \tilde{G}_{2\eta}^{(2)}, \quad (24a)$$

$$\tilde{G}_{2\eta\eta}^{(2)} + \frac{1}{2}f\tilde{G}_{2\eta}^{(2)} + f'\tilde{G}_2^{(2)} - \frac{1}{2}g\tilde{F}_2^{(2)} = 0 \quad (24b)$$

Given that there are no region 1 terms at $O(\xi^{-1}\ln\xi)$ the boundary conditions are, simply that

$$\tilde{F}_2^{(2)}(0) = 0, \quad \tilde{G}_2^{(2)}(0) = 0, \quad \text{and}$$
$$\tilde{F}_{2\eta}^{(2)}, \tilde{G}_2^{(2)} \to 0 \quad \text{as} \quad \eta \to \infty \quad (24c)$$

Equations (24) are satisfied by the eigensolutions

$$\tilde{F}_2^{(2)} = \lambda(\eta f' - f), \quad \tilde{G}_2^{(2)} = \lambda\eta g' \quad (25)$$

where λ is arbitrary. These solutions are termed leading-edge-shift eigensolutions by Daniels and Simpkins (1984), and their presence in that context is related to uncertainties in the position of the leading edge in a large-distance asymptotic theory. In the present context the presence of such an eigensolution means that the most that can be hoped for is the determination of λ because the $O(\xi^{-1})$ equations have solutions containing an arbitrary multiple of the eigensolution. At $O(\xi^{-1})$ in region 2 the equations are

$$F_{2\eta\eta}^{(2)} = G_{2\eta}^{(2)} \quad (26a)$$

$$G_{2\eta\eta}^{(2)} + \frac{1}{2}fG_{2\eta}^{(2)} + f'G_2^{(2)} - \frac{1}{2}g'F_2^{(2)} = -\frac{1}{2}\left(\frac{\kappa_2}{\kappa_1}\right)f''f'' + \lambda ff'' \quad (26b)$$

and the boundary conditions are that

$$F_2^{(2)}(0) = \frac{1}{2}\left(\frac{\kappa_2 K_1}{\kappa_1 K_2}\right)g'(0), \quad G_2^{(2)}(0) = 0, \quad \text{and}$$
$$F_{2\eta}^{(2)}, G_2^{(2)} \to 0 \quad \text{as} \quad \eta \to \infty \quad (26c)$$

Equations (26) have the solution

$$F_2^{(2)} = \frac{1}{2}\left(\frac{\kappa_2}{\kappa_1}\right)^2 f'' + \frac{1}{2}\left(\frac{\kappa_2}{\kappa_1}\right)\left(\frac{K_1}{K_2} - \frac{\kappa_2}{\kappa_1}\right) g'(0)\mathcal{F}(\eta) + \sigma(\eta f' - f) \quad (27a)$$

$$G_2^{(2)} = \frac{1}{2}\left(\frac{\kappa_2}{\kappa_1}\right)^2 f''' + \frac{1}{2}\left(\frac{\kappa_2}{\kappa_1}\right)\left(\frac{K_1}{K_2} - \frac{\kappa_2}{\kappa_1}\right) g'(0)\mathcal{G}(\eta) + \sigma\eta f'' \quad (27b)$$

where σ is arbitrary, and $\mathcal{F}$ and $\mathcal{G}$ satisfy the equations

$$\mathcal{F}_\eta = \mathcal{G}, \quad (28a)$$

$$\mathcal{G}_{\eta\eta} + \frac{1}{2} f \mathcal{G}_\eta + f'\mathcal{G} - \frac{1}{2} g' \mathcal{F} = \lambda f f'' \quad (28b)$$

with $\mathcal{F}(0) = 1$, $\mathcal{G}(0) = 0$, and $\mathcal{G}'(0) = 0$. Here λ is defined according to

$$\bar{\lambda} = \frac{1}{2}\left(\frac{\kappa_2}{\kappa_1}\right)\left(\frac{K_1}{K_2} - \frac{\kappa_2}{\kappa_1}\right) g'(0)\bar{\lambda} \quad (28c)$$

and is obtained from the requirement that $\mathcal{G} \to 0$ as $\eta \to \infty$. A straightforward application of a fourth-order Runge–Kutta shooting method code yields

$$\lambda = 0.770424 \quad (29)$$

Following from this, the region 1 solution at $O(\xi^{-3/2} \ln \xi)$ is

$$\tilde{F}_2^{(1)} = 0, \quad \tilde{G}_2(1) = \frac{1}{2}\left(\frac{\kappa_2}{\kappa_1}\right)\left(\frac{K_1}{K_2} - \frac{\kappa_2}{\kappa_1}\right) g'(0)\bar{\lambda}(1 + y) \quad (30)$$

from which the rate of heat transfer is found to be

$$Q = -g'(0) - \frac{1}{2}\left(\frac{\kappa_2}{\kappa_1}\right)\left(\frac{K_1}{K_2} - \frac{\kappa_2}{\kappa_1}\right) g'(0)\lambda \xi^{-1} \ln \xi + O(\xi^{-1}) \quad (31)$$

In Eq. (31) the $O(\xi^{-1})$ term contains σ which cannot be obtained using asymptotic methods. This means that it is difficult to use Eq. (31) to verify the numerical results, for the second and third terms will be substantially different in magnitude only when $\ln \xi$ is very large. For this problem, therefore, a detailed comparison between the numerical and asymptotic solutions is not possible. An examination of the numbers corresponding to the various curves shows that the deviation of Q from $-g'(0)$ decays roughly like ξ^{-1} (as opposed to any other power of ξ), and this gives some qualitative verification of the theory. A more substantial confirmation lies in the fact that when regions 1 and 2 have identical properties, the above expression for Q must reduce to that of the self-similar boundary layer. In this case $K_1 = K_2$ and $\kappa_1 = \kappa_2$ and therefore the logarithmic term is absent in Eq. (31).

ANALYSIS OF THE TWO-SUBLAYER CASE

In this section the numerical solution of the third section and the asymptotic solution of the fourth section are extended to cover the case where there are two sublayers adjacent to the heated surface. In nondimensional terms the heated surface is now located at $y = -2$, with region 1 lying in $-2 \le y \le -1$, region 2 lying in $-1 \le y \le 0$, and region 3 comprising the half-plane, $y \ge 0$. The respective permeabilities and diffusivities are K_1, K_2, and K_3, and κ_1, κ_2, and κ_2. We take region 3 to be the reference layer, and, to reduce somewhat the number of parameters to vary, we restrict attention to cases where regions 1 and 3 have identical properties. This means that region 2 is regarded as an imperfection in an otherwise isotropic medium.

Numerical solutions are obtained using a modified version of the Keller-box code described in the third section. All details of implementation are the same except that two interfaces need to be considered, and we use a total of 131 points in the cross-stream direction: 61 lie in region 1 as before, 20 equally spaced points are used in region 2, and the remainder comprise region 3.

In Figures 7 to 10 we show representative examples of the streamlines and isotherms for a two-sublayer model. In each case we can see the effect of the different properties of region 2. Figures 7 and 8 correspond to cases where $K_2 = 5K_3$ and $K_2 = K_3/5$ with $\kappa_1 = \kappa_2 = \kappa_3$, while Figures 9 and 10 correspond to cases where the three permeabilities are identical but $\kappa_2 = 5\kappa_3$ and $\kappa_2 = \kappa_3/5$. In Figures 7a and 8a we see clearly the effect of having a highly impermeable region 2. Near the leading edge the boundary layer develops at the normal rate until it begins to encounter region 2. The entrained fluid is able to flow upwards less easily in region 2 and this has the effect of increasing the rate of growth of the boundary layer. A boundary layer that is thick relative to the datum case will then have a decreased rate of heat transfer from the heated surface. When the developing boundary layer encounters region 3 its rate of growth decreases once more as thermal conduction normal to the surface becomes weaker relative to the effect of upwards advection. The opposite is found to be the case in Figures 7b and 8b where region 2 is relatively permeable. Here region 2 induces an increased upwards advection and hence the boundary layer grows less quickly when it first encounters the relatively permeable layer. When region 2 corresponds to a relatively highly insulating

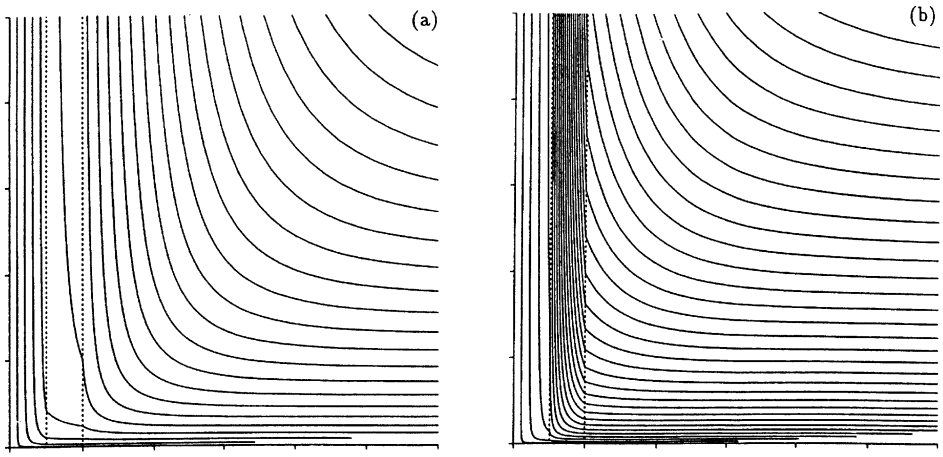

Figure 7. Streamlines for the three-layer configurations given by $\kappa_1 = \kappa_2 = \kappa_3$, $K_1 = K_3$, and (a) $K_2 = 0.2K_3$, (b) $K_2 = 5K_3$. The tick-marks on the axes are again at intervals of length 2. The two interfaces are depicted as dashed lines.

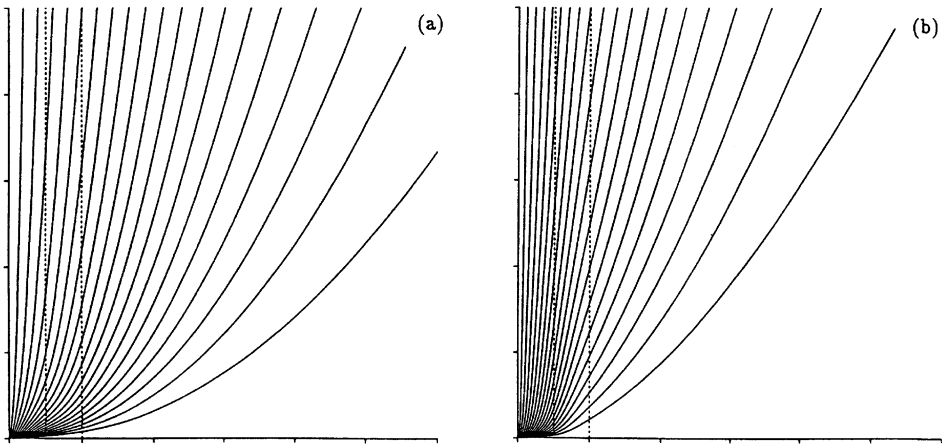

Figure 8. Isotherms corresponding to the cases shown in Fig. 7.

layer the effect in terms of the rate of growth of the boundary layer is the same as when it is relatively permeable. This is seen by comparing Figures 8b and 9a with the datum case. The detailed shapes of the streamlines and isotherms are considerably different when comparing these cases, but the qualitative results are again similar in terms of the boundary layer thickness and rate of heat transfer. This is also true of the case where region 2 is relatively conducting (Fig. 9b) when compared with a highly impermeable region 2 (Fig. 8a).

The evolution of the rate of heat transfer with ξ at the heated surface is shown in Figs. 11 and 12. Figure 11 shows the effect of having different values of K_2 on the rate of heat transfer, while Figure 12 corresponds to the effect of having different values of κ_2. The deviation of Q away from $-g'(0)$ takes place over a relatively short interval in ξ when K_2/K_1 is small or when κ_2/κ_1 is large. This fact appears to be related to the relatively fast growth of the boundary layer in these cases. When the boundary layer grows slowly then the variation of Q also takes place relatively slowly.

The prediction of the rate of heat transfer at asymptotically large values of ξ follows in almost exactly the same way as in the last section. Therefore we shall only quote

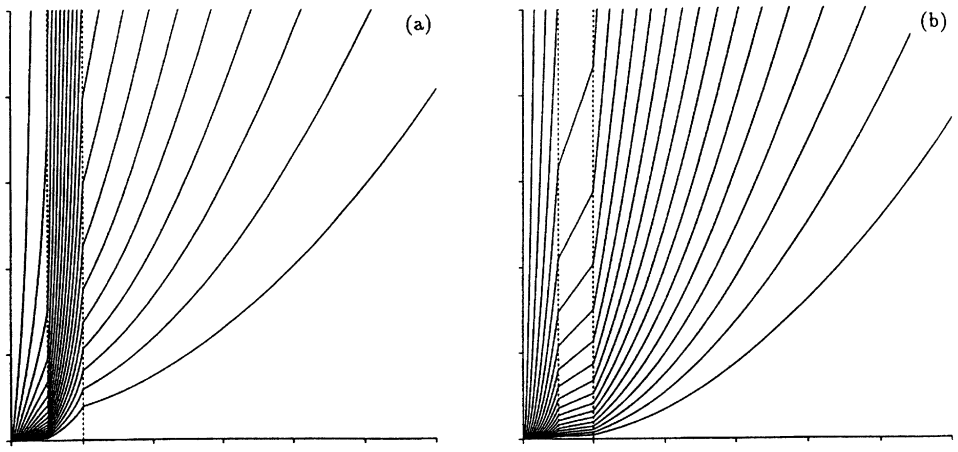

Figure 9. Isotherms for the three-layer configurations given by $K_1 = K_2 = K_3$, $\kappa_1 = \kappa_3$, and (a) $\kappa_2 = 0.2\kappa_3$, (b) $\kappa_2 = 5\kappa_3$.

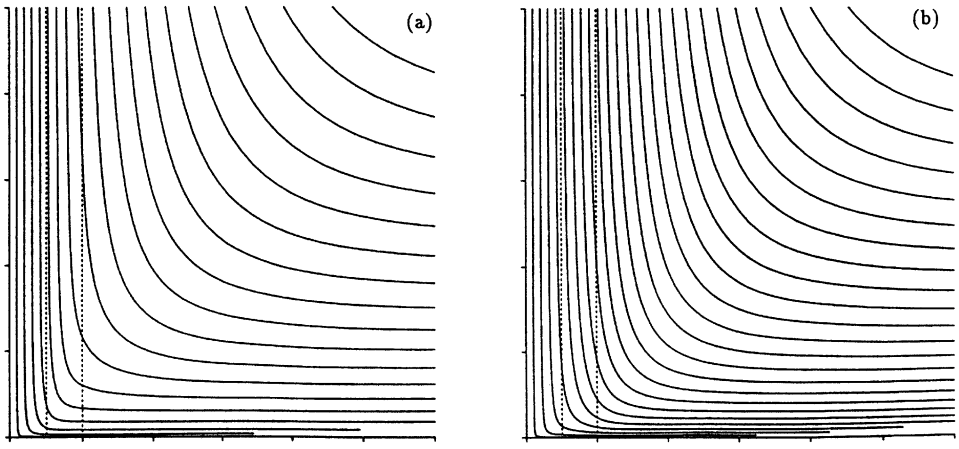

Figure 10. Streamlines corresponding to the cases shown in Fig. 9.

the results we have obtained. The basic asymptotic expansion takes the form

$$F^{(1)} = \xi^{-1/2}F_1^{(1)} + \xi^{-1}F_2^{(1)} + \xi^{-3/2}\ln\xi\tilde{F}_3^{(1)} + \xi^{-3/2}F_3^{(1)} + \ldots \quad (32a)$$

$$G^{(1)} = 1 + \xi^{-1/2}G_1^{(1)} + \xi^{-1}G_2^{(1)} + \xi^{-3/2}\ln\xi\tilde{G}_3^{(1)} + \xi^{-3/2}G_3^{(1)} + \ldots \quad (32b)$$

$$F^{(2)} = \xi^{-1/2}F_1^{(2)} + \xi^{-1}F_2^{(2)} + \xi^{-3/2}\ln\xi\tilde{F}_3^{(2)} + \xi^{-3/2}F_3^{(2)} + \ldots \quad (32c)$$

$$G^{(2)} = 1 + \xi^{-1/2}G_1^{(2)} + \xi^{-1}G_2^{(2)} + \xi^{-3/2}\ln\xi\tilde{G}_3^{(2)} + \xi^{-3/2}G_3^{(2)} + \ldots \quad (32d)$$

$$F^{(3)} = f(\eta) + \xi^{-1/2}F_1^{(3)} + \xi^{-1}\ln\xi\tilde{F}_2^{(3)} + \xi^{-1}F_2^{(3)} + \ldots \quad (32e)$$

$$G^{(3)} = g(\eta) + \xi^{-1/2}G_1^{(3)} + \xi^{-1}\ln\xi\tilde{G}_2^{(3)} + \xi^{-1}G_2^{(3)} + \ldots \quad (32f)$$

In regions 1 and 2 we have the following leading order solutions,

$$F_1^{(1)} = \frac{K_1}{K_3}(y+2), \quad G_1^{(1)} = \frac{\kappa_3}{\kappa_1}g'(0)(y+2) \quad (33a)$$

$$F_1^{(2)} = \frac{K_2}{K_3}(y+1), \quad G_1^{(2)} = \frac{\kappa_3}{\kappa_2}g'(0)(y+1) \quad (33b)$$

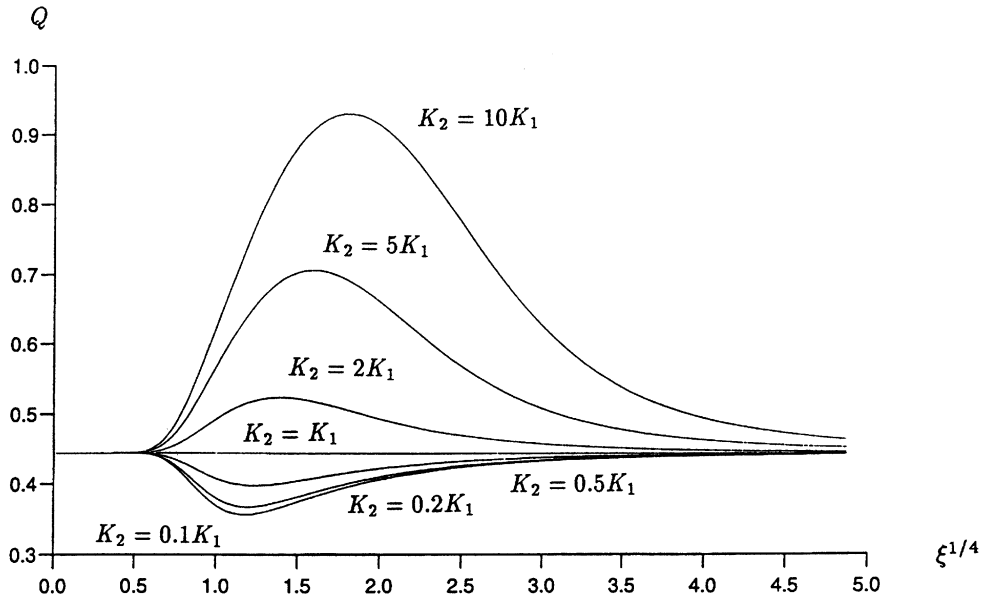

Figure 11. Values of Q for different permeability ratios with $\kappa_1 = \kappa_2 = \kappa_3$.

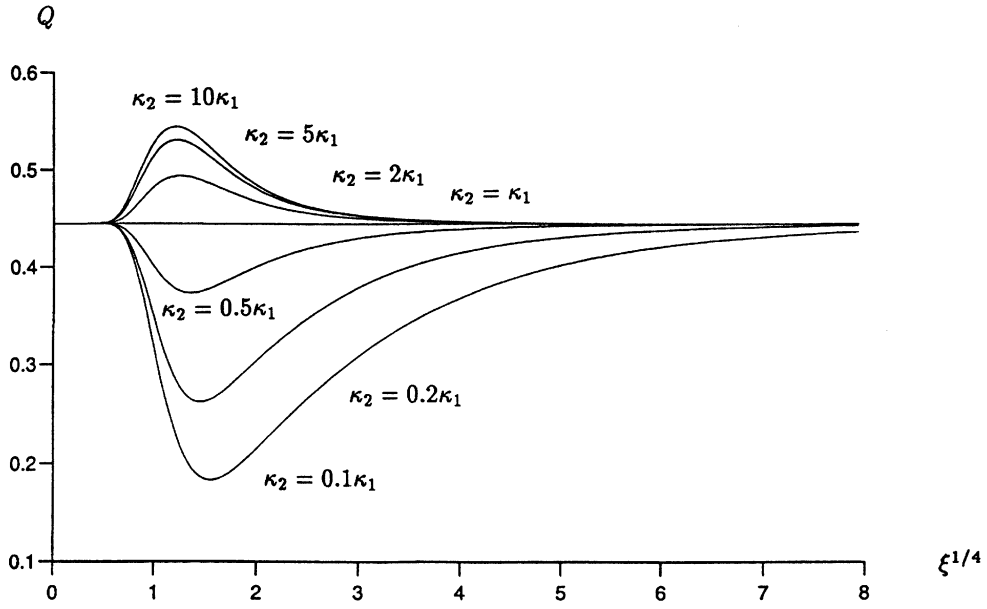

Figure 12. Values of Q for different diffusivity ratios with $K_1 = K_2 = K_3$.

while in region 3 we have

$$F_1^{(3)} = \frac{K_1 + K_2}{K_3} + \kappa_3\left(\frac{1}{\kappa_2} + \frac{1}{\kappa_3}\right)(g(\eta) - 1),$$

$$G_1^{(3)} = \kappa_3\left(\frac{1}{\kappa_2} + \frac{1}{\kappa_3}\right)g'(\eta) \tag{33c}$$

The next terms in regions 1 and 2 are

$$F_2^{(1)} = \frac{1}{2}\left(\frac{K_1\kappa_3}{K_3\kappa_1}g'(0)\right)(y+2)^2, \quad G_2^{(1)} = 0 \tag{34a}$$

$$F_1^{(2)} = \frac{1}{2}g'(0)\frac{\kappa_3}{K_3}\left[\frac{K_2}{\kappa_2}(y+1)^2 + 2\frac{K_2}{\kappa_1}(y+1) + \frac{K_1}{\kappa_1}\right],$$

$$G_2^{(2)} = 0 \tag{34b}$$

At this point we need again to consider eigensolutions. At $O(\xi^{-3/2} \ln \xi)$ in region 3 the solution is

$$\tilde{F}_2^{(3)} = \lambda(\eta f' - f), \quad \tilde{G}_2^{(3)} = \lambda\eta g' \tag{35}$$

where λ is obtained by requiring that the $O(\xi^{-3/2})$ equations have a solution. This condition yields

$$F_2^{(3)} = \frac{1}{2}\left[\kappa_3\left(\frac{1}{\kappa_1} + \frac{1}{\kappa_2}\right)\right]^2 f'' + \omega g'(0)\mathcal{F}$$

$$+ \sigma(\eta f' - f) \tag{36a}$$

$$G_2^{(3)} = \frac{1}{2}\left[\kappa_3\left(\frac{1}{\kappa_1} + \frac{1}{\kappa_2}\right)\right]^2 f''' + \omega g'(0)\mathcal{G} + \sigma\eta g' \tag{36b}$$

$$\lambda = \omega\bar{\lambda} \tag{36c}$$

where σ is again arbitrary, $\bar{\lambda}$ is given by Eq. (29), $\mathcal{F}$ and $\mathcal{G}$ satisfy Eq. (28a,b), and ω is given by

$$\omega = \frac{\kappa_3}{\kappa_2}\left(\frac{K_2}{K_3} - \frac{\kappa_3}{\kappa_2}\right) + 2\frac{\kappa_3}{\kappa_1}\left(\frac{K_2}{K_3} - \frac{\kappa_3}{\kappa_2}\right) + \frac{\kappa_3}{\kappa_1}\left(\frac{K_1}{K_3} - \frac{\kappa_3}{\kappa_1}\right) \tag{37}$$

The logarithmic terms in regions 1 and 2 are, therefore

$$\tilde{F}_2^{(1)} = 0, \quad \tilde{G}_2^{(1)} = \frac{\kappa_3}{\kappa_1}\lambda g'(0)(y+2) \tag{38a}$$

$$\tilde{F}_2^{(2)} = 0, \quad \tilde{G}_2^{(2)} = \frac{\kappa_3}{\kappa_2}\lambda g'(0)(y+2) \tag{38a}$$

Hence the rate of heat transfer is

$$Q = -g'(0) - \omega\bar{\lambda}g'(0)\xi^{-1} \ln \xi + O(\xi^{-1}) \tag{39}$$

Once more we see that the expression for the rate of heat transfer reduces to that of the uniform medium when $K_1 = K_2 = K_3$ and $\kappa_1 = \kappa_2 = \kappa_3$.

THE MULTIPLY LAYERED POROUS MEDIUM

Consider now the case of a porous medium composed of an infinite set of constant-width layers. Attention is focused on those cases for which the layers have alternating properties. In the numerical study the layers, in addition, have identical thicknesses, but this restriction is relaxed for the asymptotic analysis.

At this point we assume that the layers each have nondimensional thickness, 1, with region i lying between $y = i - 1$ and $y = i$, and where the heated surface is at $y = 0$. The odd-numbered layers have permeability K_1 and diffusivity κ_1, which are regarded as the reference values. The even-numbered layers have permeability K_2 and diffusivity κ_2. The flow in this system is obtained numerically by a further modification of the Keller-box method; now the code is able to solve for cases with a large number of interfaces. In region 1 we take 61 points as before, and either 10 or 20 further intervals per layer were found to provide a sufficiently accurate solution. We shall consider cases where $K_2 > K_1$ with $\kappa_1 = \kappa_2$, and where $\kappa_2 < \kappa_1$ with $K_1 = K_2$. The former cases were run with 20 intervals per sublayer, whereas the latter used 10 intervals to avoid poor numerical conditioning of the Jacobian matrix. In both cases solutions were obtained over 20 sublayers and integration proceeded to $\xi = 20$ in sufficiently small steps. The cases were chosen because the boundary layers obtained are sufficiently narrow to fit well into the computational domain. Test cases were run for other parameter cases and the proximity of the outer y boundary affected adversely the accuracy of the solutions near $\xi = 20$.

Figures 13 and 14 display the respective effects on the flow and temperature fields of different values of the permeability ratio K_2/K_1 in a thermally uniform medium. Therefore we assumed that $\kappa_1 = \kappa_2$ but took the following values of the permeability ratio: 2, 5, and 10. The flow in the evenly numbered layers increases in strength as K_2/K_1 increases and the overall increase in the strength of the flow entrained by the heated surface is seen by the reduced spacing of the streamlines far from the heated surface. The decreasing width of the boundary layer commensurate with the enhanced flow as K_2/K_1 increases is seen clearly in Fig. 14. Cases where $K_2 = K_1$ and κ_2/κ_1 takes the values 0.5, 0.2, and 0.1 are shown in Figs. 15 and 16. The overall decrease in the boundary layer thickness as the diffusivity ratio decreases is consistent with previous arguments about the balance of heat conduction and heat advection. In these cases, where the diffusivity ratio decreases, unlike those above where the permeability ratio increases, the decreas-

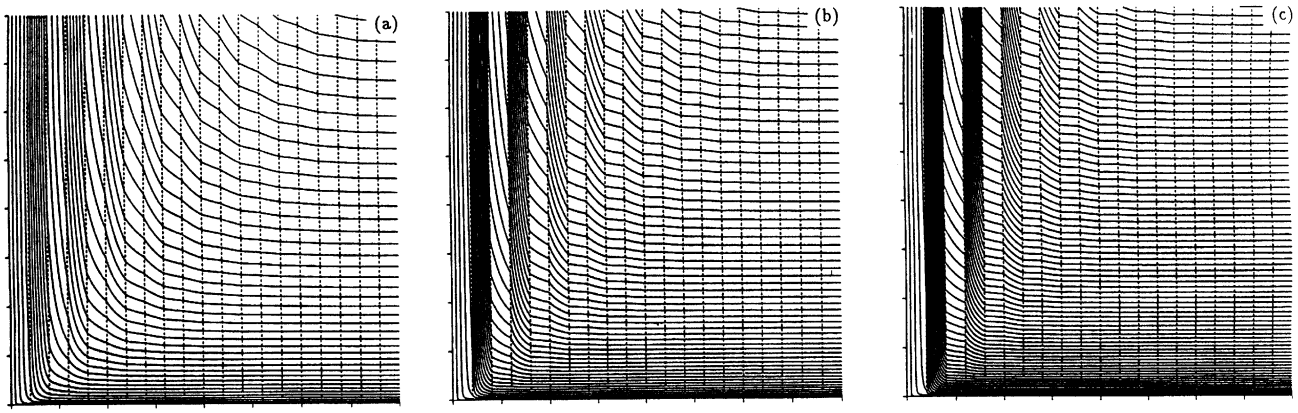

Figure 13. Streamlines for the multiply layered medium with $\kappa_1 = \kappa_2$. The cases displayed correspond to (a) $K_2 = 2K_1$, (b) $K_2 = 5K_1$, and (c) $K_2 = 10K_1$. In this figure and Figs. 14 to 16 tickmarks correspond to intervals of 2.5. The interfaces between the individual sublayers are shown as dashed lines.

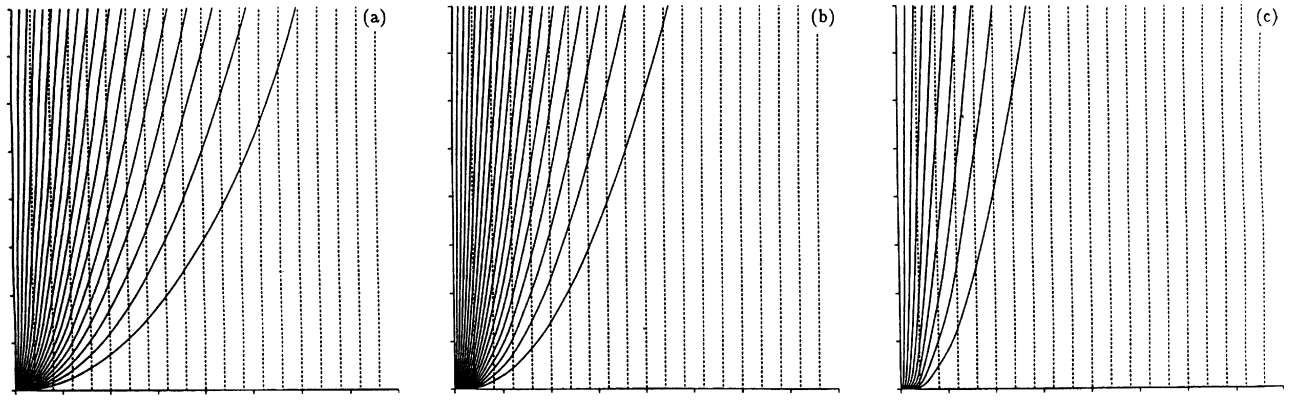

Figure 14. Isotherms corresponding to the cases shown in Fig. 13.

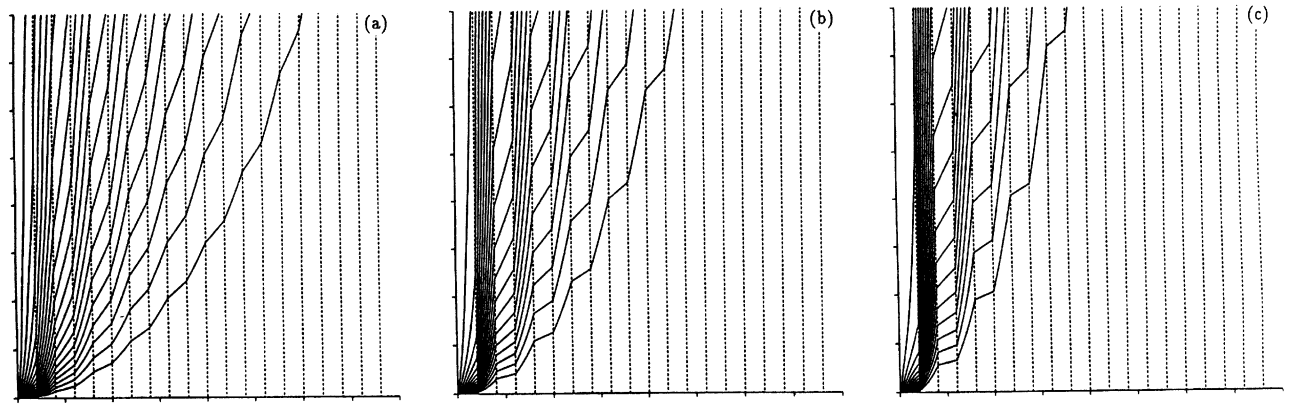

Figure 15. Isotherms for the multiply layered medium with $K_1 = K_2$. The cases displayed correspond to (a) $\kappa_2 = 0.5\kappa_1$, (b) $\kappa_2 = 0.2\kappa_1$, and (c) $\kappa_2 = 0.1\kappa_1$.

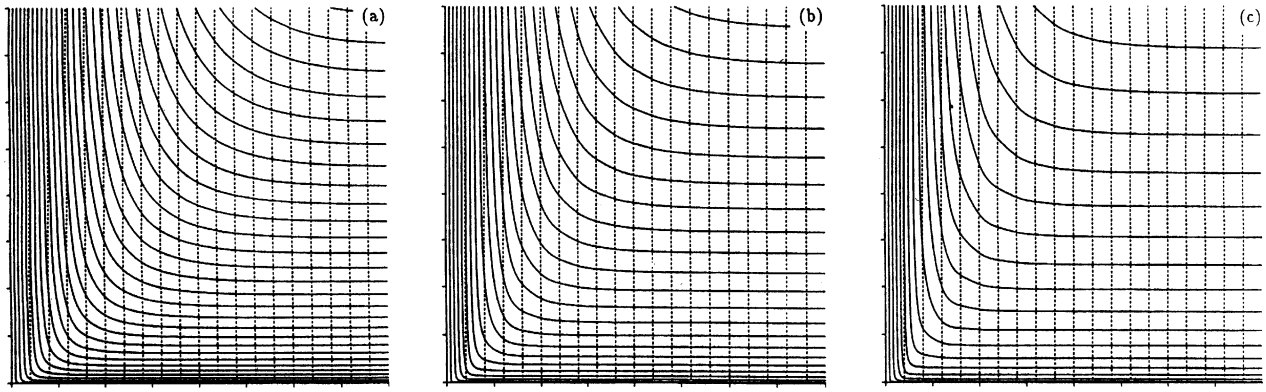

Figure 16. Streamlines corresponding to the cases shown in Fig. 15.

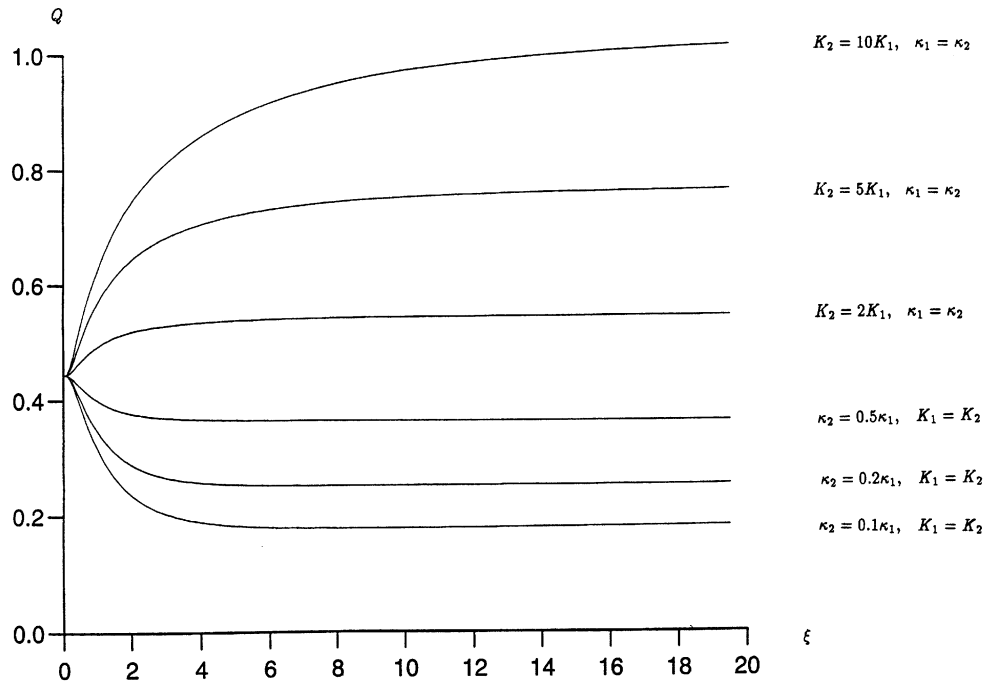

Figure 17. Values of Q for various permeability and diffusivity ratios.

ing width of the boundary layer is accompanied by a decreasing rate of entrainment into the boundary layer; this is seen by the widening gap between the streamlines far from the heated surface as shown in Fig. 16. A summary of these flows is given in Fig. 17, which shows the evolution of the rate of surface heat transfer with ξ. Near the leading edge the value of Q is independent of the permeability and diffusivity ratios, but the eventual growth of the boundary layer into and beyond region 2 modifies this. The approach to an asymptotic value seems to take place remarkably quickly where, for the case $\kappa_2 = 0.1\kappa_2$, $K_1 = K_2$, the rate of heat transfer has essentially attained its asymptotic value at $\xi = 6$, and this corresponds to the boundary layer being contained within only about six layers.

We turn now to the asymptotic analysis for large values of ξ. This turns out to have a very different form to that

presented earlier because of the layering of the entire medium. Far from the leading edge the boundary layer is substantially thicker than the sublayer widths and this fact will be used as a basis for the analysis. Here we assume that the odd-numbered layers have nondimensional thickness 1 while the even-numbered layers have thickness δ.

When ξ is large the boundary layer width is $O(\xi^{1/2})$ in terms of y but the sublayer widths are $O(1)$. In terms of the usual similarity variable, $\eta = y/\xi^{1/2}$, the boundary layer thickness is $O(1)$ while the sublayer widths are $O(\xi^{-1/2})$, an asymptotically small value. Given this latter point the asymptotic analysis will proceed by solving the governing equations using the sublayer widths themselves as the numerical steplength. In particular, we shall solve the numerical problem analytically over two adjacent layers and compare the result with that of a uniform medium.

In layer i the equations are

$$F_{\eta\eta}^{(i)} = \left(\frac{K_1}{K_{\text{ref}}}\right) G_\eta^{(i)} \tag{40a}$$

$$\left(\frac{\kappa_1}{\kappa_{\text{ref}}}\right) G_{\eta\eta}^{(i)} + \frac{1}{2} F^{(i)} G_\eta^{(i)} = \xi(F_\eta^{(i)} G_\xi^{(i)} - F_\xi^{(i)} G_\eta^{(i)}) \tag{40b}$$

and the interface conditions to be applied between this layer and the next are

$$F^{(i)} = F^{(i+1)}, \quad K_2 F_\eta^{(i)} = K_1 F_\eta^{(i+1)}, \quad G^{(i)} = G^{(i+1)},$$
$$\kappa_1 G_\eta^{(i)} = \kappa_2 G_\eta^{(i+1)} \tag{41}$$

Here i is taken to be odd so that the analysis can be applied beginning with layer 1 at the heated surface. We retain the generality of not specifying which layer is the reference layer. We also assume that all ξ-derivatives are negligible at leading order; this is a valid assumption that is shown to be true when considering the next terms in the asymptotic expansion. Hence the ith layer has thickness $\xi^{-1/2}$ while the $(i+1)^{\text{st}}$ layer has thickness $\xi^{-1/2}\delta$. In the first instance we shall use Euler's method as this is relatively easy to present and illustrates well the general principles involved. We now reduce Eqs. (40) to first-order form where the right-hand side is set to zero, as per the above assumption. Let

$$F^{(i)} = a^{(i)}(\eta), \quad F_\eta^{(i)} = b^{(i)}(\eta), \quad G^{(i)} = c^{(i)}(\eta), \quad \text{and}$$
$$G_\eta^{(i)} = d^{(i)}(\eta), \tag{42}$$

Hence these new variables satisfy the equations

$$a_\eta^{(i)} = b^{(i)} \tag{43a}$$

$$b_\eta^{(i)} = \left(\frac{K_1}{K_{\text{ref}}}\right) d^{(i)} \tag{43b}$$

$$c_\eta^{(i)} = d^{(i)} \tag{43c}$$

$$d_\eta^{(i)} = \left(\frac{\kappa_{\text{ref}}}{\kappa_1}\right)\left(-\frac{1}{2} a^{(i)} d^{(i)}\right) \tag{43d}$$

One step of length $\xi^{-1/2}$ gives the following in region i:

$$a^{(i+1)} = a^{(i)} + \xi^{-1/2} b^{(i)} \tag{44a}$$

$$b^{(i+1)} = b^{(i)} + \xi^{-1/2}\left(\frac{K_I}{K_{\text{ref}}}\right) d^{(i)} \tag{44b}$$

$$c^{(i+1)} = c^{(i)} + \xi^{-1/2} d^{(i)} \tag{44c}$$

$$d^{(i+1)} = d^{(i)} + \xi^{-1/2}\left[-\frac{1}{2}\left(\frac{\kappa_{\text{ref}}}{\kappa_I}\right) a^{(i)} d^{(i)}\right] \tag{44d}$$

These are the values of the four variables in region i, but at the interface with region $i+1$. On applying the interface conditions [Eq. (41)], they become

$$a^{(i+1)} = a^{(i)} + \xi^{-1/2} b^{(i)} \tag{45a}$$

$$b^{(i+1)} = \left(\frac{K_I}{K_1}\right) b^{(i)} + \xi^{-1/2}\left(\frac{K_I}{K_{\text{ref}}}\right) d^{(i)} \tag{45b}$$

$$c^{(i+1)} = c^{(i)} + \xi^{-1/2} d^{(i)} \tag{45c}$$

$$d^{(i+1)} = \left(\frac{\kappa_I}{\kappa_2}\right) d^{(i)} + \xi^{-1/2}\left[-\frac{1}{2}\left(\frac{\kappa_{\text{ref}}}{\kappa_2}\right) a^{(i)} d^{(i)}\right] \tag{45d}$$

in region $i+1$, but at the same interface. The use of Euler's method with one step of length $\xi^{-1/2}\delta$ will take us to the interface with the next layer, and the application of the appropriate interface conditions yields the following expressions for the four variables at the start of region $i+2$:

$$a^{(i+2)} = a^{(i)} + \xi^{-1/2}\left(\frac{K_1 + \delta K_2}{K_1}\right) b^{(i)} + \xi^{-1}\delta\left(\frac{K_2}{K_{\text{ref}}}\right) d^{(i)} \tag{46a}$$

$$b^{(i+2)} = b^{(i)} + \xi^{-1/2}\left(\frac{K_i}{K_{\text{ref}}}\right)\left(\frac{\kappa_2 + \delta\kappa_1}{\kappa_2}\right) d^{(i)} + \xi^{-1}\delta\left(\frac{K_1 \kappa_{\text{ref}}}{K_{\text{ref}} \kappa_2}\right)\left(-\frac{1}{2} a^{(i)} d^{(i)}\right) \tag{46b}$$

$$c^{(i+2)} = c^{(i)} + \xi^{-1/2}\left(\frac{\kappa_2 + \delta\kappa_1}{\kappa_2}\right) d^{(i)} + \xi^{-1}\delta\left(\frac{\kappa_{\text{ref}}}{\kappa_2}\right)\left(-\frac{1}{2} a^{(i)} d^{(i)}\right) \tag{46c}$$

$$d^{(i+2)} = d^{(i)} + \xi^{-1/2}\left(\frac{\kappa_{ref}}{\kappa_1}\right)\left(\frac{\kappa_2 + \delta\kappa_1}{\kappa_2}\right)\left(-\frac{1}{2}a^{(i)}d^{(i)}\right)$$

$$+ \xi^{-1}\delta\left[\left(\frac{\kappa_{ref}^2}{\kappa_1\kappa_2}\right)a^{(i)}a^{(i)}d^{(i)} - \left(\frac{\kappa_{ref}}{\kappa_2}\right)b^{(i)}d^{(i)}\right] + \ldots \quad (46d)$$

Thus we have obtained the formulae for integrating forward over one period, that is, two layers of the composite medium. It is this which we will compare with an appropriate uniform medium.

It is important to note that when the above analysis is repeated using a second-order method, the $\xi^{-1/2}$ terms in Eq. (46) are recovered, but the ξ^{-1} terms are different. A third-order method would recover the $\xi^{-1/2}$ and ξ^{-1} terms of the second order analysis but not the $\xi^{-3/2}$ terms, and so on. Now if we use Eq. (46) as the numerical method for solving the full two-point boundary value ordinary differential system, then the numerical solution is first-order accurate and has an error of $O(\xi^{-1/2})$. This error is associated with the local ξ^{-1} terms in Eq. (46). The difference equations in Eq. (46) may be shown to be identical up to terms in $\xi^{-1/2}$ with those obtained by solving numerically the equations,

$$F_{\eta\eta} = \left(\frac{K_1 + \delta K_2}{(1+\delta)K_{ref}}\right)G_\eta \quad (47a)$$

$$G_{\eta\eta} = -\frac{1}{2}FG_\eta\left(\frac{\kappa_2 + \delta\kappa_1}{1+\delta}\right)\left(\frac{\kappa_{ref}}{\kappa_1\kappa_2}\right) \quad (47b)$$

using one step of length $\xi^{-1/2}$ and one of length $\xi^{-1/2}\delta$. This means that to leading order the layered medium acts like a homogeneous medium of permeability, $\bar{K}$, and diffusivity, $\bar{\kappa}$, where

$$\bar{K} = \frac{K_1 + \delta K_2}{(1+\delta)} \quad \text{and} \quad \bar{\kappa} = \frac{\kappa_1\kappa_2}{\kappa_2 + \delta\kappa_1}(1+\delta) \quad (48a, b)$$

The size of the leading order correction to the above "mean" solution is motivated by the fact that even very highly accurate numerical solutions of the basic equations [i.e., Eq. (40) with no ξ-derivatives] differ from those of Eq. (47) in the ξ^{-1} terms. This local truncation error implies a global error of $O(\xi^{-1/2})$ in the leading order asymptotic solution already found; an appropriate extension to the above analysis that obtains the next terms in the asymptotic expansion will be reported on elsewhere.

To obtain the asymptotic rate of heat transfer from the heated surface we must look in detail at the relation between $G_\eta(\eta = 0)$ found by solving numerically Eqs. (47) and the value of $d^{(1)}$ [or $G_\eta^{(i)}(\eta = 0)$] defined in Eq. (42). Hence we find that the scaled rate of heat transfer, Q, is given by

$$Q \sim \left[\frac{\kappa_2}{K_1}\left(\frac{K_1 + \delta K_2}{\kappa_2 + \delta\kappa_1}\right)\right]^{1/2} g'(0) \quad (49)$$

The values of Q obtained by the full numerical computation of the governing nonsimilar equations are shown in Fig. 17, and the asymptotic values obtained there confirm the accuracy of Eq. (49).

CONCLUSION

The purpose of this article was to consider the effect of layering on the vertical free convection boundary layer flow in a porous medium. Although this is, to our knowledge, the first time such a boundary layer analysis has been undertaken, it is necessary to mention the article by Shaw and Dawe (1984) which considers the free convection induced by a horizontal line heat source placed at the vertical discontinuity between two porous media with different properties. In that article the authors show that the flow may be analyzed using standard techniques of matched asymptotic analysis, and that leading-order nonsimilarity does not occur.

With regard to the present analysis, existing work on the stability of the boundary layer flow from a uniformly heated vertical surface embedded in an isotropic porous medium suggests that flow in a layered medium should be stable. The governing nonsimilar equations were then solved using suitably modified versions of the Keller-box method and the results were supplemented by detailed asymptotic analyses. It was found that thickness of the boundary layer and the associated rates of heat transfer are intimately dependent on the values of the permeabilities and diffusivities of the various layers. In the two-layer and three-layer configurations a detailed comparison of the asymptotic rate of heat transfer with the numerical results was hampered by the appearance of eigensolutions in the expansion. In both these configurations eigensolutions appeared in the outer region solution at $O(\xi^{-1})$, and therefore we anticipate that this will also be the case with any finite number of sublayers. When the medium is composed of an infinite number of layers an entirely different asymptotic analysis is necessary, and the leading order rate of heat transfer thus obtained shows good agreement with the numerical solutions.

It is important to note criteria governing the validity of the present analysis. We have assumed that all permeability and diffusivity ratios are $O(1)$ quantities. Should either ratio become very large or very small (specifically a power of R, for the boundary layer analysis is, strictly speaking, an asymptotic analysis as $R \to \infty$), then the present analy-

sis will need to be reworked to account for this. But very large or very small ratios which remain $O(1)$ as $R \to \infty$ (fixed values such as 100 or 0.01) will only affect the ease of obtaining numerical solutions. One referee queried the use of the boundary layer approximation in layers other than the first. The boundary layer approximation is valid whenever $y << x$ so that streamwise derivatives in the diffusion terms are negligible. Here, $y = O(1)$ and $x = (R)$ and therefore we have a boundary layer flow in all layers. The boundary layer approximation is violated when $x = O(R^{-1})$, a point extremely close to the leading edge, but this is common in boundary layer flows.

It has already been noted that the layering considered here is not the only form of layering that is possible. Interfaces that are perpendicular to the heated surface are also possible, the two main forms being those where the interfaces themselves are either horizontal or vertical. In the former case detailed asymptotic analyses near to the interface will be necessary in order to determine how the boundary layer evolves as the distance from the leading edge increases. In the latter case the resulting flow will be fully three-dimensional and therefore a two-dimensional extension of the Keller-box method will be necessary to compute the evolving boundary layer. It is hoped to report on both of these aspects in due course.

ACKNOWLEDGMENT

The author would like to thank the referees for their useful comments which have improved the quality of presentation of this article.

REFERENCES

Chang, I.-D. and Cheng, P., Matched asymptotic expansions for free convection about an impermeable horizontal surface in a porous medium, *Int. J. Heat Mass Transfer,* vol. 26, pp. 163–174, 1983.

Cheng, P. and Chang, I.-D., Buoyancy induced flows in a porous medium adjacent to impermeable horizontal boundaries, *Int. J. Heat Mass Transfer,* vol. 19, pp. 1267–1272, 1976.

Cheng, P. and Hsu, C. T., Higher order approximations for Darcian free convection about a semi-infinite vertical flat plate, *Trans. ASME J. Heat Transfer,* vol. 106, pp. 143–151, 1984.

Cheng, P. and Minkowycz, W. J., Free convection about a vertical flat plate imbedded in a porous medium with application to heat transfer from a dike, *J. Geophys. Res.,* vol. 82, pp. 2040–2044, 1977.

Daniels, P. G. and Simpkins, P. G., The flow induced by a heated vertical wall in a porous medium, *Q. J. Mech. Appl. Math.,* vol. 37, pp. 339–354, 1984.

Donaldson, I. G., Temperature gradients in the upper layers of the earth's crust due to convective water flows, *J. Geophys. Res.,* vol. 67, pp. 3449–3459, 1962.

Georghitza, St. I, The marginal instability in inhomogeneous porous media, *Proc. Camb. Philos. Soc.,* vol. 57, pp. 871–877, 1961.

Gill, A. E., A proof that convection in a porous vertical slab is stable, *J. Fluid Mech.,* vol. 35, pp. 545–547, 1969.

Hsu, C. T., Cheng, P., and Homsy, G. M., Instability of free convection flow over a horizontal impermeable surface in a porous medium, *Int. J. Heat Mass Transfer,* vol. 21, pp. 1221–1228, 1978.

Hsu, C. T. and Cheng, P., Vortex instability in buoyancy induced flow over inclined heated surfaces in porous media, *ASME J. Heat Transfer,* vol. 101, pp. 660–665, 1979.

Lai, F. C. and Kulacki, F. A., Natural convection across a layered porous cavity, *Int. J. Heat Mass Transfer,* vol. 31, pp. 1247–1260, 1988.

Lewis, S., Bassom, A. P., and Rees, D. A. S., The stability of vertical thermal boundary layer flow in a porous medium, *Eur. J. of Mech. B Fluids,* vol. 14, pp. 395–408, 1995.

Masuoka, T., Katsuhara, T., Nakazono, Y., and Isozaki, S., Onset of convection and flow patterns in a porous layer of two different media, *Heat Transfer Jpn Res.* vol. 7, pp. 39–52, 1979.

McKibbin, R., Convection in an aquifer above a layer of heated impermeable bedrock, *NZ J. Sci.,* vol. 26, pp. 49–64, 1983.

McKibbin, R., Heat transfer in a vertically-layered porous medium heated from below, *Transp. Porous Media,* vol. 1, pp. 361–370, 1986.

McKibbin, R. and O'Sullivan, M. J., Onset of convection in a layered porous medium heated from below, *J. Fluid Mech.,* vol. 96, pp. 375–393, 1980.

McKibbin, R. and O'Sullivan, M. J., Heat transfer in a layered porous medium heated from below, *J Fluid Mech.,* vol. 111, pp. 141–173, 1981.

McKibbin, R. and Tyvand, P. A., Thermal convection in a porous medium composed of alternating thick and thin layers, *Int. J. Heat Mass Transfer,* vol. 26, pp. 761–780, 1983.

McKibbin, R. and Tyvand, P. A., Thermal convection in a porous medium with horizontal cracks, *Int. J. Heat Mass Transfer,* vol. 27, pp. 1007–1023, 1984.

Nield, D. A. and Bejan, A., Convection in porous media, Springer Verlag, Berlin, 1992.

Poulikakos, D. and Bejan, A., Natural convection in vertically and horizontally layered porous media heat from the side, *Int. J. Heat Mass Transfer,* vol. 26, pp. 1805–1814, 1983.

Rana, R., Horne, R. N., and Cheng, P., Natural convection in a multi-layered geothermal reservoir, *Trans. ASME J. Heat Transfer,* vol. 101, pp. 411–416, 1979.

Rees, D. A. S., Nonlinear wave stability of vertical thermal boundary layer flow in a porous medium, *J. Appl. Math. Phys. (Z.A.M.P.),* vol. 44, pp. 306–313, 1993.

Rees, D. A. S. and Riley, D. S., The three-dimensional stability of finite-amplitude convection in a layered porous medium

heated from below, *J. Fluid Mech.,* vol. 211, pp. 437–461, 1990.

Rees, D. A. S. and Storesletten, L., The effect of anisotropic permeability on free convective boundary layers in porous media, *Transp. Porous Media,* vol. 19, pp. 79–92, 1995.

Riley, D. S. and Rees, D. A. S., Non-Darcy natural convection from arbitrarily inclined heated surfaces in saturated porous media, *Quarterly J. Mech. Appl. Math.,* vol. 38, pp. 277–295, 1985.

Shaw, D. C. and Dawe, R. A., Effects of a vertical discontinuity in a porous medium on a plane convection plume at high Rayleigh numbers, *Int. J. Heat Mass Transfer,* vol. 28, pp. 789–794, 1984.

Storesletten, L. and Rees, D. A. S., The influence of higher-order effects on the linear instability of thermal boundary layer flow in porous media, Submitted to *Int. J. Heat Mass Transfer,* vol. 4, pp. 1833–1843, 1998.

Trew, M. and McKibbin, R., Convection in anisotropic inclined porous layers, *Transp. in Porous Media,* vol. 17, pp. 271–283, 1994.